Flow process and rheology control by Ultrasound-Doppler along the food value chain from material pre-processing to gastro-intestinal digestion

Erich Windhab[1], Yasushi Takeda[1], Damien Dufour[2], Kim Mishra[1], Samsun Nahar[3] and Beat Birkhofer[4]

[1] ETH Zürich (ETH); Food Process Engineering (FPE); Schmelzbergstr.9, CH-8092 Zürich, Switzerland
[2] Ubertone, 67300 Schiltigheim, France; 14, rue du Brochet, 67300 Schiltigheim-Strasbourg, France
[3] Sheffield Hallam University, Howard Street, Sheffield S1 1WB, United Kingdom
[4] Swiss Re Risk Engineering Services, Swiss Re AG, Mythenquai 50/60, 8022 Zürich, Switzerland

Ultrasound-Doppler has proved to be a powerful in-line measuring technique for non-invasive flow mapping as well as for the characterization of complex fluid rheology in processing flows. Accordingly, it has been exemplary applied along a main part of the value chain for the manufacture of chocolate confectionery from pre-crystallization, emulsification or aeration/foaming to 3D-Printing and molding. During subsequent cooling and solidification Ultrasound attenuation measurements enabled us to characterize structure formation and detachment from the mold walls. After melting during oral processing US-Doppler measurements were readdressed for in vitro studies of the flow characteristics in the oro-gastro-intestinal processing steps of swallowing, gastric mixing/dispersing and duodenal passage. For this, functional models of the human esophagus, stomach and duodenum were designed, and characteristic flow situations explored by Ultrasound-Doppler measurements. It was demonstrated that results from such measurements complemented well to the derivation of process-structure-property (S-Pro2) relationships for each of the considered processing steps. Such allow further integration into an "S-Pro^2 cascade" from which a reverse engineering approach could be derived, thus facilitating the adjustment of targeted consumer-relevant sensory and digestion patterns. This is of interest for the development of chocolate confectionery with low calorie density and a slowed kinetics of the adjustment of the glycemic index in the blood serum phase.

Keywords: Ultrasound-Doppler, flow mapping, in-line rheometry, multiphase food dispersions, oro-gastro-intestinal processing, in vitro models, esophagus stomach and duodenum

1. Introduction

To gain an authentic insight into flow processes in which complex fluid system structures are generated or transformed due to the acting flow stresses, non-invasive in-line measurements of the velocity field are required. In case of laminar flow fields in viscous, non-Newtonian and non-transparent fluid systems Ultrasound Doppler Velocimetry (UVP) has proved to be a powerful tool to not only allow for flow mapping, but also enable in-line rheometry if rheometric flow conditions (stationery plane layer flow) are present [1]. Such exist in cylindrical pipe flow which is in general an indispensable element in flow processing plants. If the viscosity function has been measured as described before once for a certain structural steady state of a non-Newtonian fluid system, locally acting shear stresses and related viscosities acting in more complex laminar velocity fields of such fluid system (as e.g detected by US-Doppler flow mapping), can be determined [2].

With the work presented here, we wanted to exemplarily highlight the versatility of the ultrasonic Doppler technology in its application over a larger part of the value chain for the production, consumption and digestion of chocolate confectionery. Accordingly the flow processing steps of (i) pipe transport, (ii) seed and shear pre-crystallization, (iii) micro-foaming, (iv) molding/3D-printing, (v) swallowing (esophagus transport) , (vi) gastric dispersive mixing and (vii) duodenal transport by peristalsis are followed with major focus on flow mapping for (ii), (iii), (v), (vi) and (vii) and rheological measurements in cylindrical pipe flow sections for (i) before and after (ii).

2. US-Doppler in process flow analyses

2.1 Steady state in-line pipe flow rheometry

In cylindrical pipe flow at Reynolds numbers Re < 2300, the acting shear rate distribution can be calculated from the first derivative of the radial velocity distribution as:

$$\dot{\gamma}(r) = dv(r)/dr \qquad (1)$$

Since, as derived from momentum balance, the radial shear stress distribution $\tau(r)$ in laminar cylindrical pipe flow is a linear function of the radius r as well as of the acting pressure gradient dp/dx but in-dependent of the fluid rheology:

$$\tau(r) = 0.5\, r\, dp/dx \qquad (2)$$

$$\tau(r) = \eta(r)\, dp/\gamma. \qquad (3)$$

simple static pressure difference detection at the pipe wall (r = R) over a defined length dx of such pipe, gives access to the wall shear stress and the radial shear stress distribution. Based on Newton's shear stress law the fluid viscosity function is received in the shear stress range of $0 \le \tau < \tau(R)$ which in case of non-Newtonian fluids means that within a substantial shear rate range the shear rate dependent viscosity function $\eta(\gamma)$ is smartly received from steady state pipe flow [1,3]. Figure 1 shows the setup for UVPPD (**c**: UVP and USA measuring cell; **e**: UVP + pressure difference PD) in-line pipe rheometry and measured velocity profile (**a, d**) and a shear viscosity function for a non-Newtonian (shear-thinning) suspension of a chocolate confectionery palm fat with crystalline solid fat con-

tent of 3.9 wt.% (**b**). The needle-like fat crystal morphology causes the pronounced shear thinning flow behavior at rather low crystal concentration [3].

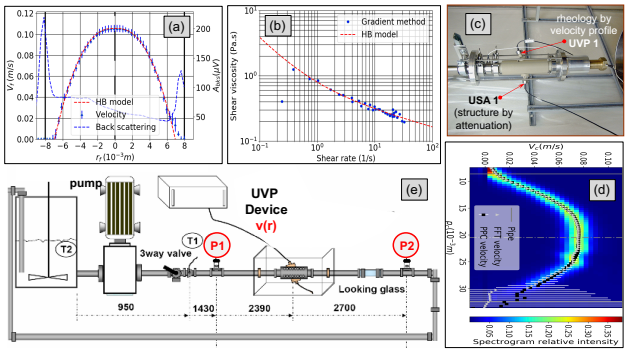

Figure 1: Velocity profile (a,d) and shear viscosity function of conventionally pre-crystallized palm fat with 3.9% SFC (NMR) at 30 kg/h mass flow rate and 26°C, measured in-line by UVP transducer (4 MHz) in experimental pre-crystallization loop schematically shown in (e) [3,4].

2.2 UVPPD rheometry in continuous crystallization process of cocoa butter / chocolate

A UVPPD measuring cell was integrated into a continuous process of cocoa butter/chocolate processing, starting with a batch pre-crystallization step (a) to adjust stable crystal $\beta_{V/VI}$ polymorph structure, followed by a 2nd continuous crystallization step in a surface scraped heat exchanger (SSHE) (b) after which the UVPPD cell (c) was placed for temperature-controlled adjustment of crystal fraction ϕ_{SFC} and related shear viscosity function $\eta(\gamma)$ (Figure 2) [5].

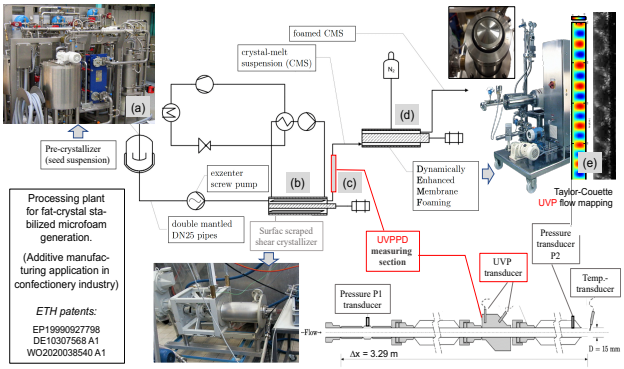

Figure 2: Processing setup for micro-foamed chocolate and fat-based filling masses consisting of: a seed-pre-crystallizer (a), an SSHE crystallizer (b), a UVPPD in-line viscosity measuring cell (c) and a Dynamically Enhanced Membrane Foaming device (d), the latter applying a Taylor-Couette flow field (e) for narrowly size distributed, stable micro-foam structure generation [5].

Figure 3 demonstrates the impact of advancing crystallization with increasing crystal fraction from ϕ_{SFC} = 1.73 to 8.8% on the UVPPD-measured velocity profiles. As has been shown by Mishra [5] for micro-foam formation the fat crystal fraction and the crystal shape are decisive for interfacial and matrix stabilization of gas bubbles thus being a prerequisite for the generation of stable but still flowable/moldable micro-foams of industrial relevance for chocolate confectionery and fat-based filling masses.

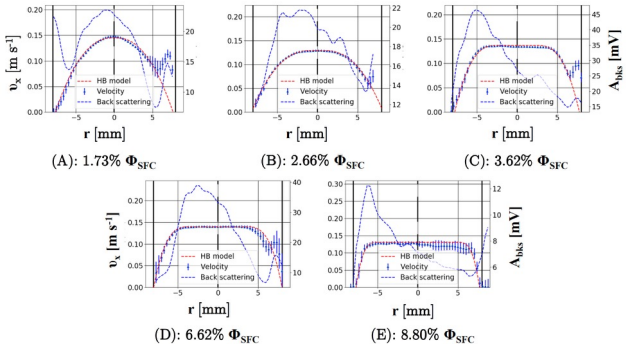

Figure 3: UVPPD-measured velocity profiles for cocoa butter crystal melt suspensions (CB CMS) crystallized at 2150s^{-1} (SSHE) in the process shown in Fig.2 with velocity scale on left y-axis and backscattering amplitude A_{bks} on the right y-axis as function of the pipe radius r [5].

2.3 UVP-flow mapping of Taylor-Couette flow in dynamic membrane foaming

A so-called Dynamically Enhanced Membrane Foaming (DEMF) device is shown in Figure 2 (d) for micro-foaming of chocolate or fat filling confectionery masses in their pre-crystallized state. In such apparatus the outer cylindrical wall of a concentric cylinder arrangement is formed by a sintermetal micro-membrane of 3 µm mean pore size. The inner cylinder is rotated between ca. 10^3-10^4 rpm thus generating high wall shear stress to detach gas bubbles of well-defined size from the membrane surface and mix them into the (pre-crystallized) fluid system which flows axially though the concentric shear gap of 0.5-5 mm width.

Axially oriented US-Doppler (UVP Duo, MetFlow) measurements allowed us to map the Taylor-Couette flow pattern under steady, wavy and modulated Taylor vortex acting conditions (see Fig. 2 (e)) and optimize gas bubble detachment from the membrane surface under adjusted oscillatory wavy Taylor vortex conditions [6].

2.4 US-attenuation measurement in molded chocolate during solidification crystallization

The application of US attenuation measurements in order to detect fat crystal networking during solidification crystallization of molded chocolate masses during continuous cooling in industrial cooling tunnels has demonstrated to allow for further viscosity and elasticity monitoring until the molded solidified product detaches from the mold wall. The latter happens as a consequence of the volume shrinkage of confectionery fats during their solidification crystallization, which is an important characteristic to enable proper demolding. Figure 4 (a) demonstrates the US-transmitter/receiver installation in a Makrolon chocolate mold and the characteristic US attenuation (US amplitude damping) pattern during chocolate mass solidification and final detachment from the mold wall. During solidification crystallization domains of initially (i) increasing viscosity and

subsequent (ii) increasing elasticity upon crystal network formation were distinguished since increase in viscosity leads to increased US-amplitude damping, whereas elasticity increase causes a reduction of the damping effect [7].

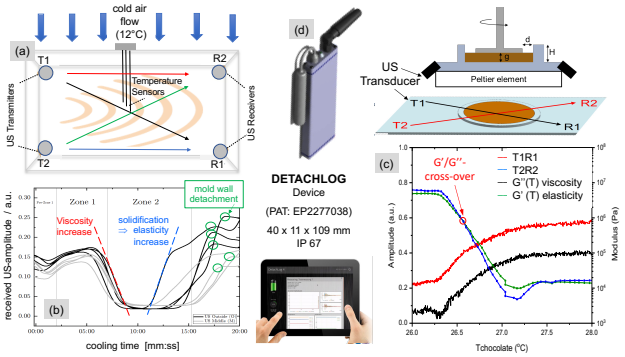

Figure 4: US-attenuation-based in-line measurement of molded chocolate solidification and mold wall detachment by ETH-Detachlog (d): (a) US transmitter/receiver placement at chocolate mold bottom; (b) US-amplitude attenuation with differentiation of viscous/elastic contributions; (c) detailed analysis of viscous and elastic moduli (G", G') during chocolate mass solidification [7].

2.5 US-Doppler flow mapping of esophagus flow during swallowing of non-Newtonian fluid

Food bolus transport through the human esophagus is caused by the peristaltic motion of the periodically collapsing elastic esophagus tube. Food after oral processing is typically in a liquid or semi-solid state with non-Newtonian rheological characteristics. In order to explore such non-Newtonian liquid food flow in a peristaltically collapsing elastic tube, an artificial esophagus was designed based on a "Sterling-resistor" flow setup as shown in figure 5 (a), in which an elastic silicon tube of 20 mm in diameter and a length of 40 cm was immersed in a water-filled transparent glass cylinder, with the entrance and exit sections of the tube being connected to inflow/outflow stainless steel pipes. Within such experimental device a transmural pressure gradient could be superimposed to the pressure gradient between entrance and exit of the elastic tube. If a critical value of the transmural pressure was exceeded the tube started to collapse. UVP-measured velocity profiles in to different degrees collapsed tubes, were in satisfying agreement with CFD simulated results. Valuable quantitative information on the significant influence of the non-Newtonian (shear thinning) rheological characteristics on esophagus flow have been gained, which are intended to be applied for development of rheology-optimized food products for elderly.

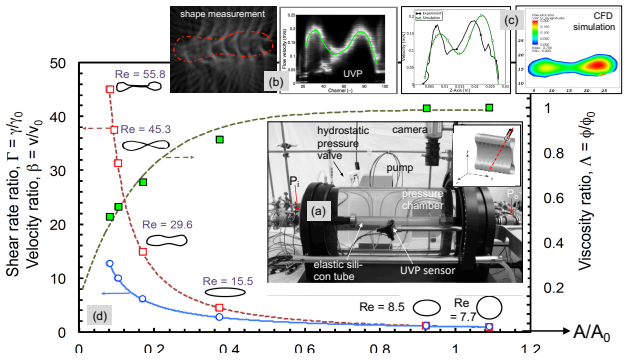

Figure 5: Experimental setup and results for artificial esophagus flow experiments in Sterling-resistor flow chamber [8]: (a) flow chamber with (i) immersed elastic silicon tube, (ii) US-Doppler transducer holder for longitudinal shift along the tube, (iii) video camera with circumferential movability for 3D-image processing of the collapsed silicon tube shape; (b) partially collapsed tube cross section and UVP detected velocity profile; (c) comparison of measured and CFD simulated velocity profiles; (d) diagram with shear rate, viscosity and mean velocity information as a function of the degree of tube collapse (expressed as cross sectional area ratio A/A_0 of the elastic tube).

2.6 US-Doppler flow mapping of gastric dispersive mixing flow

When fat continuous food systems like chocolate or fat spreads are eaten, an o/w emulsion type of 2-phase fluid system will be generated in the watery gastric juice surrounding. Depending on interfacially active components in the food and the interplay with gastric laminar and dispersive mixing, such emulsion structure can be either homogeneous or de-mixed by creaming and/or partial gelling effects. This impacts significantly on the gastric pre-digestion kinetics of the disperse fat phase with strong impact on the subsequent (final) duodenal fat digestion which in turn influences satiety.

In order to study gastric dispersive mixing flow in vitro, a functional flow model was designed for the simulation of peristaltic flow motion in the antrum. Based on fMRI images/videos the peristaltic Antrum Compression Wave (ACW) patterns were simulated.

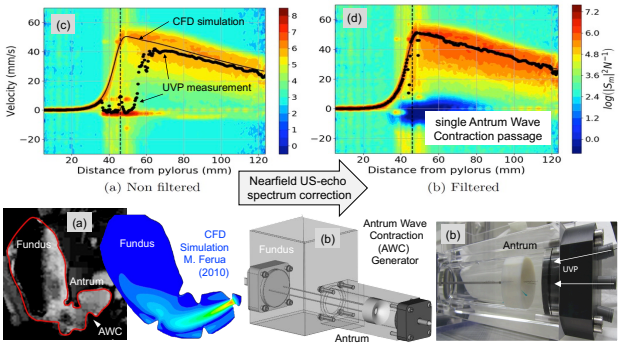

Figure 6: Flow device for in vitro testing of gastric dispersive mixing by Antrum Contraction Wave triggered flow and results from UVP flow mapping of a single ACW passage: (a) fMRI and CFD simulation as ACW study base; (b) In vitro dynamic ACW flow simulator; (c) UVP-measured velocity field in longitudinal antrum direction without "echo-correction" for the moving ACW-contour disc; (d) see (c) but with applied UVP echo correction [9].

Under the acting ACW-based dispersive mixing flow field additional simulated "fat drop" dispersing experiments were carried out and the dispersing efficiency under various ACW propagation velocity conditions and for diffe-

rent starting positions of immiscible oil droplets was systematically tested in flow experiments as well as by CFD-simulation. From these a critical dimensionless Capillary Number (Ca) was derived as denoted by equation [9],

$$Ca = \frac{R_d \tau}{\sigma} = \frac{4\eta R_d v_c RO\,(2-RO)\left[1-\frac{\delta_{apex}}{R(1-RO)}\right]^{\epsilon}}{\sigma R\,(1-RO)^3} \quad (4)$$

with R_d (drop diameter), v_c (antrum wave velocity = v_{ACW}), RO (relative occlusion = 1-Di/Da), δ_{apex} (distance from open wave contour cross section radius Ri), a (exponent), σ = interfacial tension, η (viscosity)
Figure 7 demonstrates the dependency of the capillary number experienced by the drop as function of the drop starting position. Indicated drop break-up domains are preferably related to drop-tracks passing closer to the wave contour wall and experiencing Ca-numbers ≥ ca. 0.12 (according to definition in eq. 4).

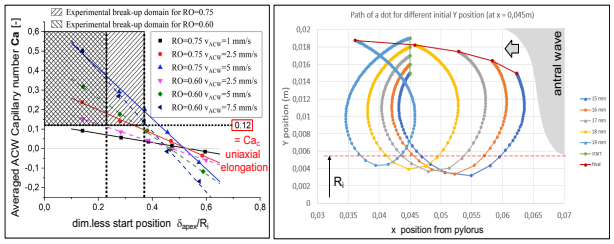

Figure 7: left: Critical Ca-number domain as a function of the starting drop position (δ_{apex}/R_i), the relative opening size of the wave contour cross section (OR) and the ACW propagation velocity (v_{ACW}); right: droplet tracks in the ACW flow field (CFD simulation) depending on the drop starting position [9].

More efficient dispersing of the fat droplets in the gastric ACW flow field, being dominated by a repulsive jet flow directed backwards from the pilorus and with high elongation rates (ε. up to ca. 5 s^{-1}) and shear rates (γ. up to ca. 10 s^{-1}), leads to the generation of an enlarged specific surface area of the oil drops which in turn leads to faster digestion in the duodenum under the action of lipolytic enzymes.

2.7 US-Doppler flow mapping of duodenal peristalsis driven intestinal juice flow

In the human small intestine, the transport of partially digested food suspensions is driven by peristaltic wave motion and /or segmentation contraction of the intestinal wall. In order to also access such flow authentically for optimized experimental in vitro simulation of digestive flow mechanisms, another "intestinal" flow device was designed as demonstrated in Figure 8. A silicon tube was immersed in a tempered transparent water bath of 1.20m in length and dynamically contracted by three roller pairs moving along the tube, with a UVP transducer connected to the roller suspension in order to keep the relative position to one selected of the roller pairs fixed, but adjustable to be directed either normal to the crest or trough section of the deformed elastic silicon tube. Flow mapping was carried out with an 8 MHz UVP transducer placed at different Positions after the roller pairs 1-3 and for different roller velocities along the tube in the range of 3 - 10 mm/s, adapted to physiological conditions of the peristaltic motion of the human small intestine (Fig. 8) [10].

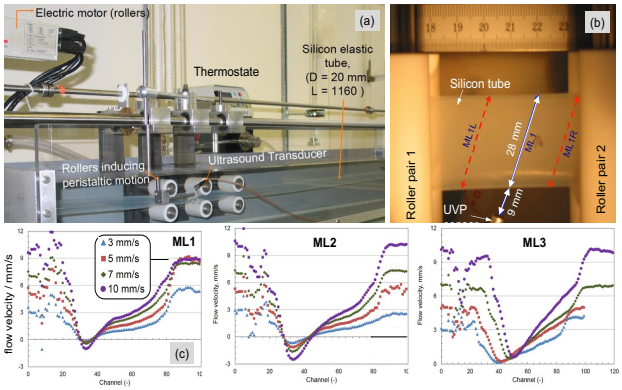

Figure 8: Small intestinal peristaltic flow testing devise with (a) intestinal tube, three contraction roller pairs and mounted UVP transducer (fixed to roller suspension, flexible for different measurement directions in the tube flow (b); (c) exemplary measured tube flow velocity profiles after each of the roller pairs (ML1-ML3) in left to right roller motion with UVP fixed in "trough" position [10].

The insight gained into experimentally approximated intestinal flow patterns will be applied for improved in vitro digestion simulation under authentically adapted flow field and flow stress conditions which impact on mixing and food structure disintegration.

3. Summary

The US-Doppler technology was approved to be a valuable tool for in-line non-Newtonian rheology measurements in rheometric pipe flow as well as for flow mapping of more complex flow situations along the chocolate confectionery food value chain from production to consumption and digestion. New insights gained into physiological flow conditions will serve for the optimization of sensory and nutritionally optimized food products.

References

[1] Windhab, E. J (1995). Rheology in food processing, chapter 5, pp. 80–116. Springer US, Boston, MA, 1995.
[2] Ouriev, B., Windhab E. (2004); Measurement Science and Technology, 14(11):1963-1972, 2004.
[3] Birkhofer, B., S. A. Jeelani, E. Windhab, B. Ouriev, J. Lisner, P. Braun, Y. Zeng (2007), Flow Measurement & Instrumentation, 19:163–169, 2007.
[4] J Wiklund, B Birkhofer, S Jeelani, M Stading, E Windhab (2012); Appl. Rheol. 22 (2012) 42232
[5] K. Mishra, D. Dufour, E. Windhab (2020); Crystal Growth & Design, 20(2):1292–1301, 2020.
[6] Pokorny L., Kohler L., Takeda Y., Windhab E. (2016); Flow Measurement and Instrumentation; 52, pp.137-143
[7] E. Windhab et al. (2012); Patent Nr. EP2277038
[8] Nahar S., Jeelani, S., Windhab, E. (2012); Chemical Eng. Science, 75:445–455, 2012.
[9] Dufour D. (2018; Dissertation ETH Zürich Nr. 24851
[10] S. Nahar, B. N. Dubey, E. J. Windhab (2019); Phys. Fluids 31, 101905 (2019); https://doi.org/10.1063/1.5123182